tvst

Article

Disease Progression in Patients with Autosomal Dominant Retinitis Pigmentosa due to a Mutation in Inosine Monophosphate Dehydrogenase 1 (IMPDH1)

Lea D. Bennett[1], Martin Klein[2], Finny T. John[1], Bojana Radojevic[1], Kaylie Jones[2], and David G. Birch[2,3]

[1] Department of Ophthalmology, University of Oklahoma Health Sciences Center, Oklahoma City, OK, USA
[2] Retina Foundation of the Southwest, Dallas, TX, USA
[3] Department of Ophthalmology, UT Southwestern Medical Center, Dallas, TX, USA

Correspondence: Lea D. Bennett, University of Oklahoma Health Sciences Center, 608 Stanton L. Young Blvd., Oklahoma City, OK, 73040, USA. e-mail: lbennett@ouhsc.edu

Received: December 9, 2019
Accepted: February 10, 2020
Published: April 23, 2020

Keyword: IMPDH1; adRP; clinical outcomes; disease progression

Citation: Bennett LD, Klein M, John FT, Radojevic B, Jones K, Birch DG. Disease progression in patients with autosomal dominant retinitis pigmentosa due to a mutation in inosine monophosphate dehydrogenase 1 (IMPDH1). Trans Vis Sci Tech. 2020;9(5):14, https://doi.org/10.1167/tvst.9.5.14

Purpose: Mutations in the inosine monophosphate dehydrogenase 1 (IMPDH1) gene are a common cause of inherited retinal degeneration (IRD). Due to species- and tissue-dependent expression of IMPDH1, there are no appropriate models of human *IMPDH1* disease. Therefore, a limited understanding remains of disease expression and rates of progression for IMPDH1-related IRD.

Methods: We evaluated semiautomated kinetic and chromatic static perimetry, spectral-domain optical coherence tomography (SD-OCT), and ultra-wide field fundus images with autofluorescence in a cohort of 12 patients (ages 11–58 at first visit). Ten patients had longitudinal data for which rates of progression were estimated.

Results: Visual acuities were relatively stable over time and the photoreceptors within the central retina remained intact. Perifoveal photoreceptor loss measured over a period of years coincided with visual fields, which were constricted and progressed over time in all patients. Rod sensitivity showed a similar pattern of defect to that of the kinetic perimetry and the autofluorescence ultra-wide field imaging. Full-field electroretinograms were severely reduced and the dark-adapted rod and mixed responses were extinguished at earlier visits than the light-adapted cone responses.

Conclusions: There was variability in disease severity at the first visit, but results show that the peripheral retina is more susceptible to the deleterious consequences of an *IMPDH1* mutation. Given the pattern of degeneration and the alternatively spliced isoforms of *IMPDH1*, potential interventions may consider targeting the periphery early in disease, modulating transcript expression, and/or preserving central vision at late stages of the disease.

Translational Relevance: These results inform clinical prognosis and offer evidence strategies toward therapeutic intervention.

Introduction

Inosine monophosphate dehydrogenases (IMPDH) are highly-conserved enzymes[1] found in bacteria and eukaryotes.[2] Two widely expressed isoforms in humans, IMPDH1 and IMPDH2, share enzymatic properties,[3] and 84% sequence identity.[4] IMPDH monomers have a catalytic region formed by an eight-stranded α/β barrel structure with two cystathionine β-synthase (CBS) repeats flanking the catalytic region.[3] These CBS domains are often found in proteins that bind adenine and/or guanine nucleotides. The IMPDH proteins are homotetramers that bind single-stranded nucleic acid and associate with polyribosomes, presumably mediated by the CBS domains. The role of these interactions is unknown, but they putatively function in RNA and/or DNA metabolism, replication, transcription, and/or translation. IMPDH1 catalyzes the synthesis of xanthine monophosphate

from inosine-5'-monophosphate with reduction of nicotinamide adenine dinucleotide.[5] This is the rate-limiting step in the de novo synthesis of guanine nucleotides.

Mutations in *IMPDH1* associated with autosomal dominant retinitis pigmentosa (adRP) are located in and around the CBS domain, but do not affect enzymatic activity or tetramer formation.[6,7] Rather, *in vitro* studies suggest that retinal degeneration is due to mutant protein misfolding and aggregation.[7] Despite the ubiquitous expression of IMPDH1, the retina is the only tissue affected by mutations in this gene.[8]

IMPDH1 is one of the top five genes most frequently linked to autosomal dominant retinitis pigmentosa (adRP), and mutations in *IMPDH1* account for 2.5% of all cases of RP.[8] IMPDH-associated adRP has phenotypically been described as an early-onset, rapidly progressing, and severe retinal degeneration with cystoid macular edema in some patients.[9–11] Best corrected visual acuity (BCVA), full-field electroretinography (ffERG), cystoid macular edema on spectral domain optical coherence tomography (SD-OCT), and kinetic visual fields have been previously reported from patients with *IMPDH1* mutations. However, changes over time in these measures, as well as dark-adapted static perimetry, photoreceptor quantification on SD-OCT, and autofluorescence on wide-field retinal images, have not been reported for this group of patients. Therefore, clinical outcome measures obtained from multiple visits were quantified to better understand disease progression and effects from a missense mutation in the gene *IMPDH1*.

Methods

Patients were recruited from six pedigrees with *IMPDH1*-associated RP. Data from previous visits were available from two clinical sites, the Retina Foundation of the Southwest in Dallas, TX, and the Dean McGee Eye Institute (DMEI) at the University of Oklahoma Health Sciences Center in Oklahoma City, OK. Informed consent was obtained. All procedures were approved by institutional ethics review boards and adhered to the Declaration of Helsinki.

Clinical Procedures

At DMEI, BCVA was measured with a traditional Snellen chart whereas Retina Foundation of the Southwest used the Electronic Visual Acuity Tester (Jaeb Center for Health Research, Tampa, FL, USA). The eye with the lower acuity, or the right eye if there was no difference between the two eyes, was dilated (tropicamide 1% and phenylephrine 2.5%) and patched for at least 30 minutes to allow dark adaptation. During dark-adaptation, the better-seeing eye was tested with kinetic perimetry for all patients. The dark-adapted eye was tested with dark-adapted static perimetry and ffERG. After functional testing, retinal imaging was performed in both eyes.

Spectral Domain Optical Coherence Tomography

The SD-OCT measures were obtained with a commercial device (Spectralis Heidelberg retina angiography + OCT; Heidelberg Engineering, Inc.). Automatic real-time registration was used with a mean of 100 scans for high-resolution images. All scans had a quality index greater than 25 dB. When available, serial scans were used where images were captured with the aid of automatic registration so that the same scan placement was used on each test. Ellipsoid zone (EZ; junction of inner and outer segments of photoreceptors) measured with the SD-OCT software was compared among visits.

Fundus and Wide-field Imaging

Fundus and wide-field imaging were assessed by one of the authors (F.T.J.). Images were acquired with the Optos camera (Optos PLC, Dunfermline, UK) to obtain pseudocolored and autofluorescence retinal images. Using the green laser (532 nm) on the Optos, scans were obtained to assess the neural retina and retinal pigmented epithelial (RPE) layers. Hyper-autofluorescence (hyper-AF; dying) and hypo-AF (dead or blocked light due to debris) gave insight into retinal health and were compared with psychophysical testing.

Perimetry

Kinetic perimetry was performed using an Octopus900 (Haag-Streit AG, Switzerland). For the Octopus900 kinetic exam, the field was mapped using spot sizes V-4e, III-4e, and I-4e at a speed of 4°/sec. Visual field area was computer-calculated for each isopter.

Dark-adapted static sensitivity to a cyan (505 nm) stimulus throughout the visual field was measured on a dark-adapted chromatic (DAC) perimeter (Medmont International Pty Ltd; Victoria, Australia).[12,13] Results were reviewed to determine whether unequivocal rod function was measured for each point, which was determined a priori as sensitivity > 30 dB.[14–21] When sensitivity to the cyan stimulus was < 30 dB, the point was retested with the red stimulus while the patient was still dark-adapted.[12] The difference in sensitivity

Table 1. Demographics

Study ID	Family ID	Ethnicity	Sex	Age at First Visit	Diagnosis
P1	UTAD045	AI/W/NH	Male	11	adRP
P2	UTAD045	AI/W/NH	Female	14	adRP
P3	UTAD045	AI/W/NH	Male	14	adRP
P4	UTAD045	W/NH	Female	37	adRP
P5	UTAD045	W/NH	Female	55	adRP
P6	RFS9534	W/NH	Female	19	Sporadic RP
P7	UTAD1301	W/NH	Female	31	adRP
P8	UTAD1026	W/NH	Male	22	adRP
P9	UTAD1026	W/NH	Female	49	adRP
P10	UTAD1026	W/NH	Male	43	adRP
P11	UTAD696	W/NH	Female	34	adRP
P12	RFS1236	W/NH	Female	58	adRP

ad, autosomal dominant; AI, American Indian; H, Hispanic; N, not; RP, retinitis pigmentosa; W, white.

was then used to determine which receptors mediated stimulus detection at the particular point tested. Cones detected both stimuli when sensitivity to cyan minus sensitivity to the red stimulus at the same point was < 6 dB. This value represents the ~ 6 dB difference in the maximum luminance of the cyan (12.58 cd/m^2; dynamic range ~75 dB) and red (4.64 cd/m^2; dynamic range ~45 dB) LEDs on the DAC and the fact that cones are about equally sensitive to these wavelengths. A difference between cyan and red between 6 dB and 30 dB indicated a mixed response where the rods mediated detection of the cyan and cones mediated detection of the red stimulus at that point.

Tests were administered by LDB or MK. In 2019, patients P2 through P5 were seen at DMEI by LDB who performed testing procedures. The Octopus perimeter was the same model but not the same devise used at both sites. The DAC was relocated to DMEI and therefore, the same machine used for all examinations.

Full-field Electroretinography

ffERGs were obtained with the ISCEV standard protocol.[22] The ffERG was recorded using a Burian-Allen ERG electrode (Hansen Ophthalmic Development Laboratory) on the same eye immediately after DAC perimetry while the eye was dark-adapted (DA) and fully dilated.

Statistical Analyses

Statistical analyses included descriptive and qualitative assessments for demographics and image analysis. Quantitative statistics were performed using the R (R Core Team, 2013) software. The difference between outcomes was calculated using the paired two-tailed Student *t*-test. The progression rates, defined as the difference in values obtained between the follow-up and baseline visits divided by the length of follow up, were calculated for each procedure performed over multiple visits. Significance was given as a P value < 0.05.

Results

Clinical Characteristics of the Patients with *IMPDH1* Mutations

Twelve patients from six families had a known missense mutation in the gene *IMPDH1* NM_000883.3: c.931G>A(p.Asp311Asn; Table 1). The pedigrees are shown for families UTAD045 [9,23] (P1-P5; Fig. 1A), RFS9534 (P6; Fig. 1B), UTAD1301[8] (P7; Fig. 1C), UTAD1026 (P8-P10; Fig. 1D), UTAD696 (P11; Fig. 1E), and RFS1236[9] (P12; Fig. 1F). Some family members have had clinical data presented previously, but the individuals in this work have not been evaluated, except for patient 6 (P6) who participated in a repeatability study for DAC perimetry [13] before her mutation was identified.

At the first visit, ages ranged from 11 to 58 years (mean 32 years ± 16 SD). Visual acuities ranged from 20/20 (0.0 logarithm of the minimum angle of resolution [LogMAR]) to no light perception. Multiple visits with an average of 6.1 years ± 5.4 SD of follow-up time were separated by better and worst acuity eyes (established at the first visit). The initial and most recent visits and the respective acuity data, refraction, and age are provided in Table 2. There was no change in BCVA for the better eye compared with the most recent visit

Table 2. Vision from First and Most Recent Visits

ID	Age (Years)	Better BCVA	Better LogMAR	Worst BCVA	Worst LogMAR	Refraction Better	Refraction Worst
P1	11	20/20	0.0	20/25	0.1	−3.50+2.50 × 005	−4.00+2.50 × 170
	21	20/20	0.0	20/25	0.1	−4.25+2.50 × 090	−4.75+2.75 × 082
P2	14	20/32	0.2	20/50	0.4	Contacts	Contacts
	17	20/32	0.2	20/32	0.2	− 10.75+3.00 × 100	− 11.75+3.00 × 075
P3	14	20/25	0.1	20/32	0.2	Contacts	Contacts
	17	20/25	0.1	20/25	0.1	−5.25+2.25 × 105	−5.50+1.50 × 085
P4	37	20/25	0.1	20/32	0.2	SC	SC
	40	20/20	0.0	20/20	0.0	−7.00+0.75 × 093	−7.50+0.75 × 059
P5	55	20/25	0.1	20/32	0.2	Lasik	Lasik
	58	20/25	0.1	20/25	0.1	Plano	0.00+0.25 × 066
P6	19	20/32	0.2	20/32	0.2	SC	SC
	40	20/40	0.3	20/40	0.3	−1.25+0.50 × 135	−1.75+1.00 × 035
P7	30	20/40	0.3	20/50	0.4	−5.75+0.50 × 130	+4.75+0.50 × 063
	34	20/40	0.3	20/50	0.4	−5.75+0.50 × 136	−6.50+1.50 × 069
P8	22	20/20	0.0	20/32	0.2	Lasik at 22 years	Lasik at 22 years
	28	20/25	0.1	20/25	0.1	Lasik at 22 years	Lasik at 22 years
P9	49	20/25	0.1	20/32	0.2	Lasik at 49 years	Lasik at 49 years
	54	20/25	0.1	20/25	0.1	−0.75+0.50 × 090	−1.00+0.25 × 008
P10	40	20/40	0.3	20/63	0.5	Lasik at 22 years	Lasik at 22 years
	43	20/32	0.2	20/40	0.3	Contacts	Lasik at 22 years
P11	34	20/32	0.2	20/50	0.4	Contacts	Contacts
P12	58	20/80	0.6	NLP	NA	NA	SC

BCVA, best corrected visual acuity; LogMAR, logarithm of the minimal angle of resolution; NA, not applicable; NLP, no light perception; SC, Sine correctione (without correction).

(mean change 0.0 LogMAR ± 0.1 SD). The fellow eye had a mean improvement of 1 line (-0.1 LogMAR ± 0.1 SD), which resulted in no statistical difference in acuity between eyes at the most recent visit (Table 2; $P = 0.0811$).

Macular integrity was evaluated with SD-OCT. Qualitative assessment of SD-OCT scans showed hyperreflective foci throughout the retinal layers (yellow; Figs. 2A-C). Macular edema (red arrows) was evident in five patients (P2 at age 17, Fig. 2A; P5 at age 57, Fig. 2B; P6 at age 39, Fig. 2D; and P10 at age 43). Five patients (P1 at age 20; P4 at age 39, Fig. 2C; P7 at age 33; P9 at age 49; and P12 at age 58) had posterior vitreous detachment (PVD; white arrowheads). The EZ is the hyper-reflective line that is easily discernible across a normal retina and in younger patients with RP. At age 17 years, P2 had an EZ (inset; green) that extended across the entire image. When photoreceptors in the periphery die, the ends of the EZ (green arrowhead) become visible on the SD-OCT image as illustrated on the horizontal line scan from P5 in Figure 2B (inset). Representative degenerative changes over 8 years from P6 shows progressive constriction of the EZ width over time (Fig. 2D).

Wide-field images for both eyes of 10 patients were symmetrical and the clinical descriptions are listed in Table 3. Traditional fundus photographs or a wide-field image of one eye was available for P11 and P1, respectively. Images from a 16-year-old male patient (P3) showed scalloped hypo-AF in the periphery (Fig. 3A) that was unique to this particular patient. Some features noted (to varying degrees) in this group are represented in the wide-field image of the left eye (OS) for P3 which shows mild pallor of the optic nerve head (ONH), decreased foveal light reflex (FLR), nerve fiber layer (NFL) sheen, mild vascular attenuation, and rare bone spicules in the periphery (Fig. 3A′). Dark-adapted sensitivity was reduced in the periphery, but was normal centrally (56.1–62.2 dB[13]; Fig. 3B). This pattern of normal or near-normal sensitivity in areas mapped by kinetic perimetry were evident for all 10 patients tested with the DAC. Areas

Table 3. Description of Wide-field Fundus Imaging

Study ID	Age (Years)	C/D Ratio	Optic Nerve Head	Macula	Vascular Attenuation	Bone Spicules	Autofluorescence
P1	21	0.05	Mild pallor	Mildly decreased FLR; NFL sheen	Mild	Rare	Hyper-AF outside vascular arcades; mid-periphery speckled RPE loss
P2	16	0.2	No pallor or PPA	Mildly decreased FLR	Mild	Rare	Hyper-AF in macula and nasal retina
P3	16	0.2	Mild pallor OS; no PPA	Mildly decreased FLR; NFL sheen	Mild	Rare	Peripheral hypo-AF with scalloped borders
P4	39	0.2	Moderate pallor; PPA OS	Mildly decreased FLR	Moderate	Diffuse	Hyper-AF ring in mid peripheral retina
P5	57	0.2	Moderate pallor; no PPA	Blunted FLR	Severe	Diffuse	Abnormal hyper-AF in macula
P6	40	0.1	No pallor or PPA	Blunted FLR; pigment mottling	Moderate	Diffuse	Ring of hyper-AF in peripheral macula between arcades; hypo-AF in mid-periphery outside of arcades with punched-out appearance
P7	34	0.05	No pallor	Moderately decreased FLR; pigmentary changes	Moderate	Diffuse; mild	Hyper-AF ring around macula
P8	28	0.05	No pallor; mild PPA	Mildly decreased FLR; NFL sheen	Mild	Rare	Hyper-AF in temporal macula; punched-out lesions in far periphery
P9	53	0.2	Large PPA; mild-moderate pallor	Bull's-eye pattern pigmentary changes; atrophy OS>OD	Severe	Diffuse	Bull's-eye pattern of abnormal hyper-AF OS>OD
P10	43	0.05	Temporal PPA; mild pallor	Mildly decreased FLR; slight pigmentation	Mild nasal	Rare	Not done
P11	34	0.1	Moderate pallor	Severely blunted FLR; pigmentary and atrophic changes	Severe	Diffuse	Poor quality
P12	58	0.2	Moderate pallor	Blunted FLR	Severe	Diffuse; dense	Hyper-AF in macula

C/D, cup-to-disc; FLR, foveal light reflex; NFL, nerve fiber layer; OD, right eye; OS, left eye; OU, both eyes, PPA, peripapillary atrophy

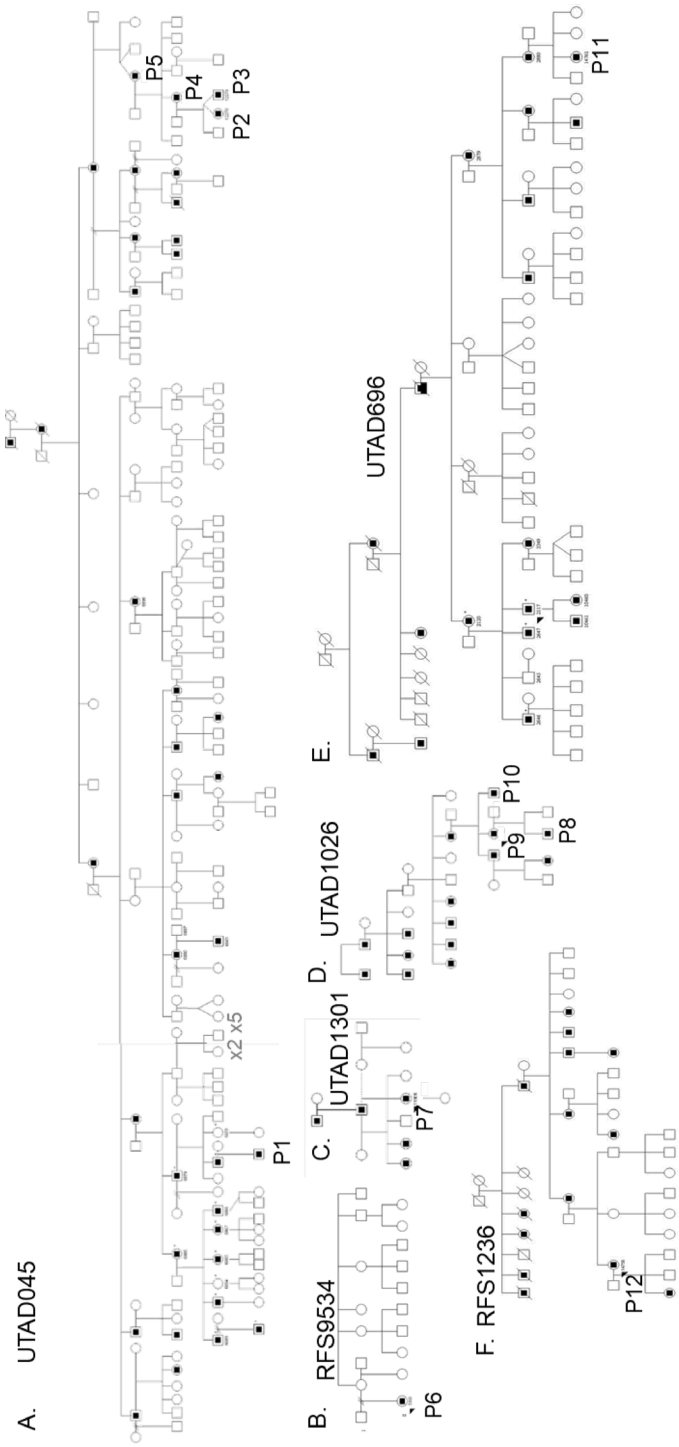

Figure 1. Family pedigrees for patients in this cohort with an *IMPDH1* mutation.

not mapped on kinetic exams had either low sensitivity (Fig. 3B, far nasal and temporal field) or were absolute scotomas (black) where the stimulus was not seen. Notice that P3 had visual field extents that were full nasally, but reduced to 45°, 50°, and 60° in the temporal field to target sizes I-4e (green), III-4e (red), and V-4e (blue; Fig. 3B′), respectively. The nasal to temporal visual field and comparative sensitivity loss were common among this cohort of patients.

The greatest ffERG amplitudes were measured in P3 at age 14 years. He had rod and mixed ffERG responses (50.1 and 121.8 µV, respectively; Fig. 3C) that were below normal (rod, 72–243 µV; mixed, 189–499 µV[24]). There were no patients with responses to rod or mixed flashes within normal range. However, P3 (Fig. 3C′) and P4 had responses to cone and 30 Hz flicker flashes that were within normal range (cone, 42–168 µV; 30 Hz flicker, 35–110 µV,[24] respectively).

Patient 1 (age 21 years) had a ring of hyper-AF that surrounded the macula just beyond the vascular arcades (Fig. 3D). Mild ONH pallor, NFL sheen, mild vascular attenuation, and rare bone spicules were also noted for P1 (Table 3). Additionally, P1 had mid-peripheral RPE loss in a speckled pattern (Arrows; Fig. 3D′). The peripheral retina showed decreased sensitivity to the DAC modulus, but there was normal sensitivity centrally (Fig. 3E). The constricted visual field to the smallest target, I-4e (green; Fig. 3E′), recapitulated the central hyper-AF observed in the wide-field image. Although the response to the ffERG rod flash was < 3.0 µV (Fig. 3F, top), the mixed flash elicited a 38.7 µV response (bottom panel). P1 also had detectable light-adapted responses to the cone and 30 Hz ffERG flashes (Fig. 3F', top and bottom, respectively). The ffERG responses to the rod, cone, and 30 Hz flashes for P1 were 80%, 45%, and 51% below normal, respectively.

Annular hyper-AF was noted for all patients, but a more pronounced definitive ring of hyper-AF was evident as the leading edge of degeneration approached the macula like the ring of hyper-AF found on images for P7, a 33-year-old female patient (Fig. 3G). Additionally, P7 had diffuse, but mild, bone spicules in the periphery, ONH drusen (inset), moderately decreased FLR, pigmentary changes in the macula, and moderate vascular attenuation (Fig. 3G′, Table 3). The central and nasal field showed near-normal DAC sensitivity, but the stimulus was not detected in the periphery (Fig. 3H). The visual fields were decreased to 20° to all targets tested (Fig. 3H′) and were similar to the constricted hyper-AF observed on the wide-field AF image (Fig. 3G). Despite the limited dark- and light-adapted visual fields, P7 had severely reduced, but measurable, responses to all ffERG flashes (Fig. 3I and 3I′). The rod response was 79% below normal and the mixed response was 74% below normal. The cone responses were reduced by 47% and 54% compared with normal responses to the cone and 30 Hz flicker ffERG flashes, respectively.

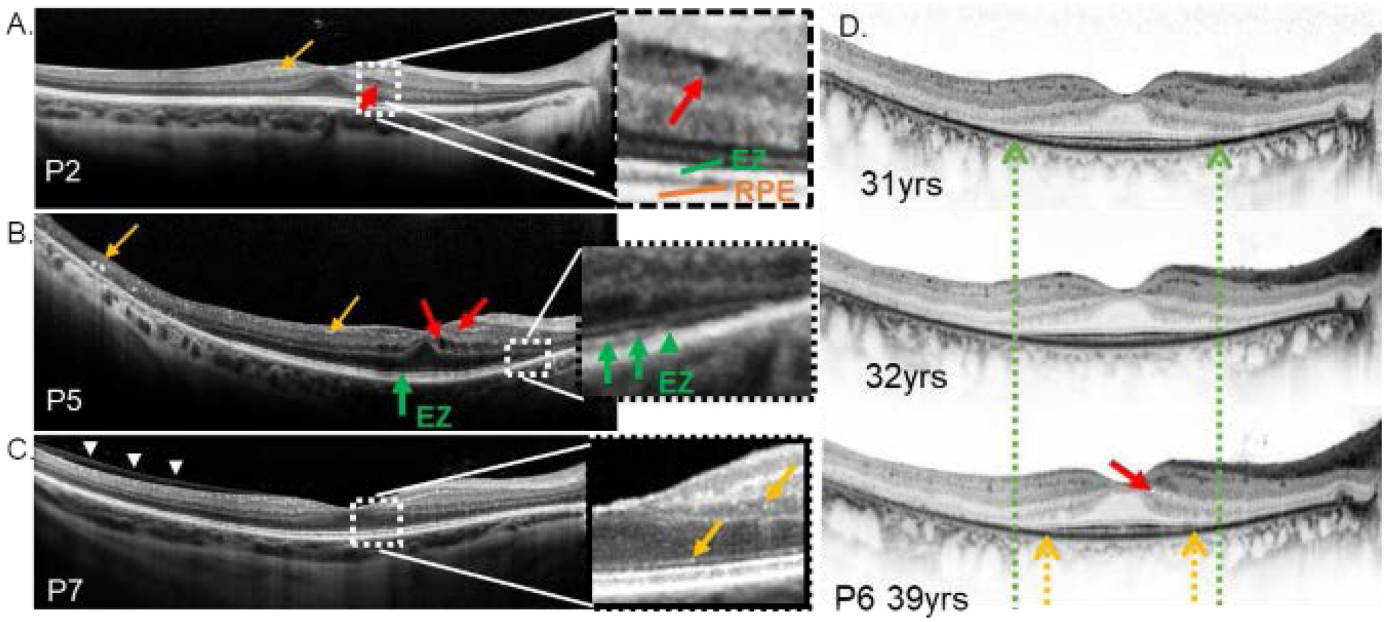

Figure 2. Degenerative changes on spectral domain optical coherence tomography (SD-OCT) images. Findings from SD-OCT scans showed hyperreflective foci (yellow arrows; A-C), macular edema (red arrows; A, B, D), and posterior vitreous detachment (PVD; white arrowheads; C). Insets highlight the ellipsoid zone (EZ) line (green; A and B), retinal pigmented epithelium (RPE; orange; and A) the end of the EZ line (green arrowhead; B). (D) EZ line regression over eight years demonstrated by the difference in length at age 31 years (green arrows) and at 39 years (yellow arrows) for P6.

Table 4. Kinetic Perimetry First and Last Visits

ID	I4e (Degree^2 First/Last)	III4e (Degree^2 First/Last)	V4e (Degree^2 First/Last)	Years Between Visits
P1	1438/1297	5900/6081	10,113/9641	5
P2	1673/384	2429/2030	3258/2627	3
P3	4833/3862	5753/5123	6602/5657	3
P4	2420/1978	2949/2936	3464/3467	3
P5	346/257	513/461	570/542	2
P6	86/89	1029/836	2037/1574	7
P7	823/538	1177/918	1362/1130	2
P8	3391/2160	8627/4920	10,772/8657	5
P9	165/ND	218/175	299/246	5

ND, not done.

Longitudinal Changes

Most patients in this group had concentric retinal degeneration (Fig. 3) that progressed from the periphery with minimal to no macular involvement until late stage of disease. Atypical presentation of change over time is shown from the right eye for P8 in Figure 4. Fundus AF imaging acquired at age 27 showed mild peripapillary hypo-AF and a hyper-AF ring surrounding the macula (Fig. 4A). The color fundus photo of the right eye showed decreased FLR, NFL sheen, vascular attenuation, and rare bone spicules in the far periphery (Fig. 4B). At a previous visit (age 22), kinetic perimetry revealed deficits to target size I-4e (green) in the temporal field, but the extents of visual field were full to targets V-4e (blue) and III-4e (red; Fig. 4C). At age 28, the nasal retina deteriorated further, as evidenced by the scotomas mapped with spot size III-4e in the temporal visual field (red; Fig. 4D).

There were eight other patients with kinetic visual field serial data. Computer-calculated isopters for first and last visits are provided in Table 4. The follow-up time ranged from 2 to 7 years with a mean of 4 years ± 1.6 SD. Altogether, visual field extents were constricted

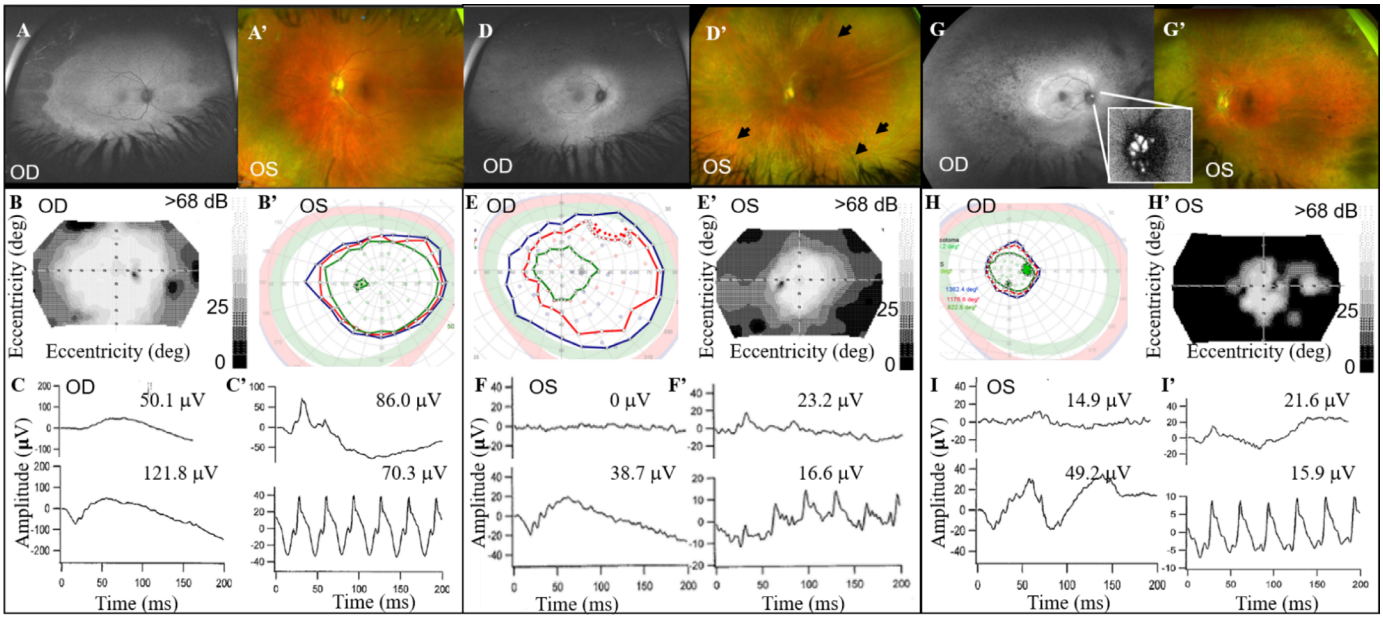

Figure 3. Patients had wide-field images that corresponded to dark-adapted sensitivity and light-adapted visual fields. (A) Right eye (OD) autofluorescent (AF) images for P3. (A′) Color fundus picture of the left eye (OS) for P3. (B) DAC sensitivity measured OD and (B′) kinetic perimetry measured OS. The arrows point to the blind spot. (C) Full-field electroretinography (ffERG) responses evaluated OD to the rod (top) and mixed (bottom) flashes. (C′) Light adapted ffERG responses to the cone and 30 Hz flicker flashes. (D) Wide-field AF image OD and (D′) color fundus photo OS for P1. (E) Kinetic perimetry was performed OD and (E′) DAC was performed OS. (F) Dark- and (F′) light-adapted ffERG responses for P1 measured OS. (G) Wide-field AF image OD and (G′) color fundus photo OS for P7. Inset, optic nerve head drusen. (H) Kinetic perimetry was performed OD and (H′) DAC was performed OS. (I) OS dark- and (I′) light-adapted ffERG responses for P7.

at an average rate of 4.6% ± 3.5 SD (V-4e target), 4.7% ± 3.3 SD (III-4e target), and 8.7% ± 6.2 SD (I-4e target) per year in this cohort.

The rate of photoreceptor degeneration was determined with SD-OCT scans from a subset of seven patients (P1, P5, P6, P7, P8, P9, and P10) who had measurable EZ. The average follow-up time was 4.2 years ± 2.6 SD; range 1.9 to 8.1 years. The loss per year on horizontal line scans was not different between better (-0.17 mm per year ± 0.12 SD) and worst (-0.14 mm per year ± 0.12 SD) seeing eyes ($P = 0.4568$). Overall, the lateral extent of the EZ decreased 3.68 % ± 2.13 SD per year for this subgroup of patients.

Only four patients (P2, P3, P4, and P8) had a 1-year follow-up visit with DAC examinations. By comparing sensitivity to red at the same locations, rod-mediated detection of the cyan stimulus was confirmed. Changes over 1 year were found with DAC perimetry for all four patients that mimicked their kinetic visual field changes. For example, reduced sensitivity from rod (blue) to cone (red)-mediated detection of the DAC stimuli was quantified for P8 in the peripapillary/temporal field at ages 27 (Fig. 4E) and 28 (Fig. 4F), respectively. This occurred at the level of hypo-AF observed on the wide-field image (Fig. 4A) and similar to the mapped scotomas (Figs. 4C and 4D). Despite the decline in light- and dark-adapted vision for P8, the ffERG responses showed little decline in five years (Fig. 4G). There were eight additional patients with longitudinal ffERG (range 1 to 8 years; mean 3.2 years ± 2.6 SD). Compared with amplitudes measured at the first visit rod, mixed, cone, and 30 Hz cone responses were reduced by 18 % ± 32 SD, 6% ± 17 SD, 5% ± 8 SD, and 11% ± 13 SD, respectively, per year.

Discussion

Here we found a relatively consistent phenotype from unrelated pedigrees that included patients who had the *IMPDH1* mutation, c.931G>A (p.Asp311Asn). Similar to previous reports,[8–10,25] the patients in this cohort had attenuation of the retinal vessels, pallor of the optic nerve, bone spicule pigmentation, RPE atrophy, restricted visual fields, decreased ffERG responses, and some had macular edema. Decreased BCVA associated with macular edema was formerly described for patients with a mutation in *IMPDH1*.[9,10] Here, edema was evident on SD-OCT (Fig. 2, red arrows) for three patients that coincided with a reduction in acuity at the same visit.

Hyperreflective foci identified on SD-OCT imaging have been observed in patients with age-related

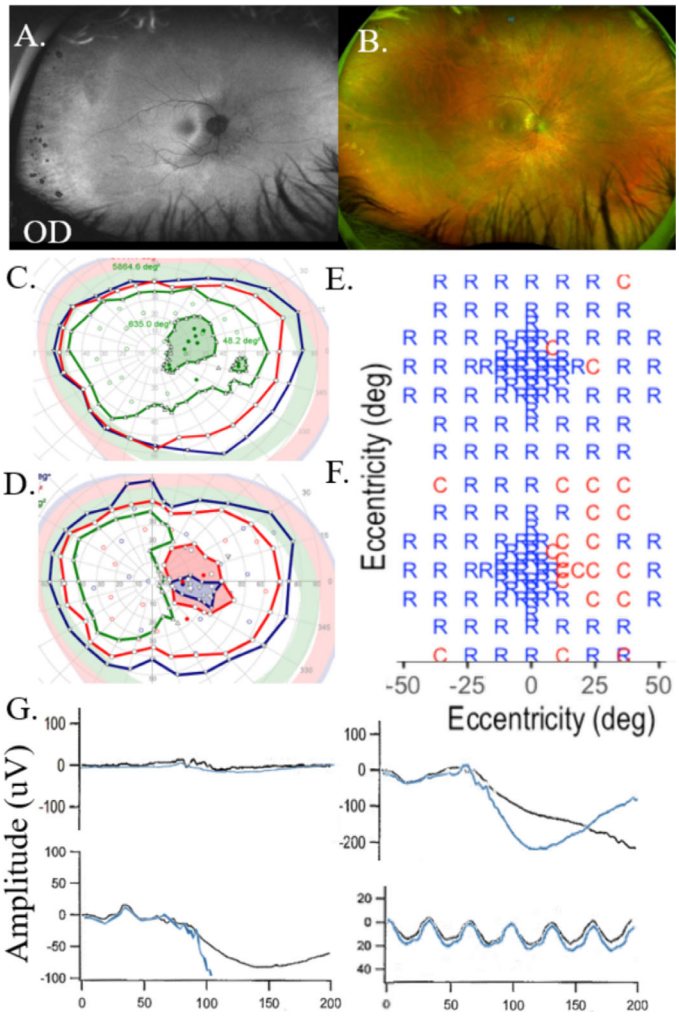

Figure 4. Right eye changes. (A) An autofluorescence image and (B) a color fundus photo of the right (OD) eye of P8 at age 27 years. (C) Visual fields OD were mapped at age 22 years to target sizes i-4e (green), III-4e (red), and V-4e (blue), and (D) at age 28 years. Dark-adapted chromatic perimetry OD with changes in rod- (blue) and cone- (red) mediated detection of the stimulus from (E) age 27 to (F) age 28 years for P8. (G) At ages 22 (black traces) and 27 years (blue traces), the full-field electroretinography responses OD were comparable for the rod (left, top), mixed (left, bottom), cone (right, top), or 30 Hz flicker (right, bottom) flashes.

macular degeneration,[26] diabetic retinopathy,[27,28] and RP.[29,30] The foci in age-related macular degeneration and diabetic retinopathy are believed to reflect macrophages, migrating RPE cells, and extravasated lipoproteins.[31] The hyperreflective foci in RP[29] were different from those described in other retinal degenerative diseases and were distributed in the inner and outer nuclear layers (INL, ONL) and subretinal space. Kuroda et al.[30] reported that patients with RP who had a disrupted EZ on SD-OCT also had hyperreflective foci in the ONL, whereas those with a healthy RPE showed no hyperreflective foci in the ONL. Moreover, patients with advanced RP who had disrupted RPE also had more of the foci.

Larger foci, like those in P5 (Fig. 2B), have been described as the activation of Müller cells, migration of activated microglia, and/or the synaptic remodeling of horizontal and amacrine cells.[30,32–34] The RPE layer on the SD-OCT image was intact for P5 in the peripheral macula where the large hyperreflective foci were located, but there were also no discernable photoreceptor layers in that area, which would support a remodeling or migrating of glial or inner retinal cells as opposed to pigment migration.

PVD has not been previously reported specifically for patients with an *IMPDH1* mutation, but are common among many forms of retinal degenerative processes. P1, P4, P7, and P11 had vitreous syneresis (liquefaction), which has been shown to precede PVD.[35] Therefore, close monitoring of patients with adRP associated with *IMPDH1* may promote early detection and timely repair should they develop a retinal detachment secondary to PVD.

The average reduction in the width of EZ among patients with RP has been reported to be 95 to 219 µm per year.[36,37] Here we determined that the EZ decreased on average 140 to 170 µm per year, which is between the rates reported for patients with autosomal recessive RP (arRP; -128 µm per year) and X-linked RP (XLRP; -219 µm per year).[38] Other forms of dominant RP typically progress at a slower rate (-95 µm per year)[38] than do XLRP or arRP. However, the rapid rate of degeneration in our cohort was not surprising and was commensurate with early onset and advanced progression, similar to XLRP and arRP. In this regard, the EZ could be designated as a primary outcome measure evaluating disease progression since the rate of change is quantifiable and measurements would likely be consistent in a clinical trial setting where images are evaluated through a reading center with experienced graders. Although we did not have images where the ends of the EZ were evident for all patients, this could be overcome by using a wide (55°) lens or by splicing multiple images together with overlapping points for alignment. Given the reduced and concentric visual fields, there is little doubt that the ends of the EZ line could have been imaged in this cohort. Thus, future studies should include trained photographers who have experience locating and capturing each end of the EZ on SD-OCT images in patients with RP.

Optic disc drusen has been reported in patients with RP,[39] Usher syndrome,[40] Alagille syndrome,[41] and Best vitelliform macular dystrophy.[42] Optic nerve head drusen (ONHD) are acellular hyaline deposits of calcium, amino and nucleic acids, and mucopolysac-

charides, believed to be a derivative of degenerated retinal ganglion cells (RGCs).[43] Complications from ONHD may include neovascularization, central retinal arterial or venous occlusion, or anterior ischemic optic neuropathy,[43] none of which were found in the four patients who had ONHD in the present study. Another complication from ONHD is visual field loss resulting from the mechanical stress on RGC axons within the ONH. This is in-line with the advanced loss of visual fields for P7 (Fig. 3G). It is difficult to know whether ONHD leads to a more severe phenotype or if ONHD develops secondary to advanced retinal degeneration because all four patients with ONHD in the present study were in advanced stages of adRP. Therefore, a natural history study enrolling a larger cohort with and without ONHD will be important to understand disease progression and determining clinical outcome measures prior to treatment trials involving patients with *IMPDH1*-related RP.

Peripapillary atrophy is the loss of RPE and choriocapillaris adjacent to the disk and has been associated with glaucoma and myopia.[44] Myopic changes affect the biomechanics of the peripapillary sclera, which is the main stress-bearing tissue of the eye. The optic discs with greater myopic deformation could accelerate the RGC axonal loss and consequently lead to VF damage.[45] Therefore, the atypical hemi-field loss for P8 could have occurred secondary to myopia-related changes (Fig. 4). This cannot be known for certain because P8 had Lasik surgery before visits analyzed in this study, and there were no prior refractive data in his chart. However, the SD-OCT image revealed a steeply curved retina indicating an elongated axial length similar to a highly myopic eye.

Mid-peripheral scotomas commonly mapped in patients with RP were for the most part absent from this population. Visual fields for P7, P9, P10, P11, and P12 were reduced to the central field at the first visit, so it is unclear whether these individuals had the same pattern of field loss over time. Previously, family UTAD045 was reported to have visual fields that were constricted by age 40 to less than 20° estimated by static perimetry.[9] Although not directly comparable to the kinetic fields presented here, our results agree with Kozma et al.[9] in that we also found severe constriction because of degeneration of the peripheral retina. However, we did have 2 patients (P4 and P10) whose visual fields were 30° and 45° at ages 40 and 47, respectively, to target size III4e. We also show that the kinetic visual fields closely resembled the AF images. Longitudinal assessment was limited because there were only multiple AF images for P2-P4 with a year between visits. Longitudinal quantification of the hyper-AF ring may be informative as a marker for disease progression for patients with an *IMPDH1* mutation.

Bowne and associates[8] reported early symptoms of constricted visual fields and comparable reductions in ffERG responses. In another study, Kozma et al.[9] demonstrated ffERG rod responses that were more severely affected than cone responses at all stages of the disease. Similarly, Wada et al.[11] also found more rod than cone reductions in the ffERG of patients with the Asp311Asn mutation. From the patients tested in the present study, the reduced ffERG responses remained consistently low when measured at different visits over time. The only ffERGs not measurable were from P9 at age 49 and P5 at age 56. Compared with patients with XLRP due to an *RPGR* mutation, we found equal loss of rod and cone ERG responses.[46] This is different from mutations in genes expressed in rods but not cones such as *RHO* mutations that cause adRP. In these patients, the rod ERG amplitudes are primarily diminished compared with the cone responses. Altogether, patients with an *IMPDH1* mutation and adRP are more similar in their ERG responses to patients with *RPGR*-related XLRP than to patients with adRP and a *RHO* mutation.[47] We do not believe ffERG would be an informative outcome measure in treatment trials for *IMPDH1*-related RP because response amplitudes are severely reduced and did not change over 1 year's time. We found 5% to 18% reduction per year in this cohort, which is far below the 35% to 50% variability previously determined for ffERG responses.[48]

IMPDH1 messenger RNA expression in the retina is approximately 10 times the average levels found elsewhere in the body,[49] indicating that retinal tissue has a unique requirement for IMPDH1. Further, Bowne et al.[50] found that *IMPDH1* expression was higher in the peripheral retina, which may explain the peripheral-to-central degeneration demonstrated here for P1, P2, P3, P4, P5, P7, and P10. However, we downloaded public dataset PRJNA369687; GEO: GSE94437[51] and did not find statistical differences in human macula versus peripheral retina *IMPDH1* transcript expression. Rather, this dataset revealed that due to alternative splicing, an *IMPDH1* variant (V7) was expressed in the human macula but not in the peripheral retina. The c.931 mutation in this cohort is located in exon 7, which is spliced from the messenger RNA and not present in V7. The c.931 mutation would be in all transcripts in the periphery compared with the macula which expresses transcripts with and without exon 7. Perhaps less mutant protein in the macula (due to V7 transcript expression) explains the early preservation of the central vision until late stage of disease.

The varying proportions of alternatively expressed *IMPDH1* transcripts suggests an opportunity for

regulation depending on the physiological needs or state of the tissue. Perhaps a metabolic regulation of *IMPDH1* expression could explain the different transcripts between the retina and other tissues. Indeed, Huang et al.[52] recently showed elevated guanosine nucleotides along with an upregulation of biosynthetic IMPDH enzymes in a subset of patients with small cell lung cancer, possibly making these tumors suitable for treatment with IMPDH inhibitors. Alternatively, single-nucleotide polymorphisms in *IMPDH1* have been associated with increased chronic [53] or acute [54] graft-versus-host disease in patients receiving hematopoietic cell transplantation, and with the incidence of kidney transplant rejection.[55] These adverse events were likely due to lower responsiveness to IMPDH inhibitors used to prevent host rejection of the donor tissue, suggesting that intronic single-nucleotide polymorphisms or those within regulatory regions of *IMPDH1* could serve as directors of gene expression or alternative splicing, thereby altering transcript and subsequent protein abundance. Thus, genomic and/or metabolomic control of transcript regulation could be used for therapeutic treatment in patients with an *IMPDH1* mutation. Given the pattern of degeneration and the alternatively spliced isoforms of *IMPDH1*, potential interventions may consider targeting the peripheral retina early in disease, modulating transcript expression to down-regulate mutation-containing transcripts, and/or preventing the loss of central vision.

Acknowledgments

Research reported in this publication was supported by the Foundation Fighting Blindness (DGB) and the National Eye Institute of the National Institutes of Health under Award Numbers K99EY027460 (LDB), R00EYE027460 (LDB), US4GM104938 (LDB), and EY09076 (DGB). The content is solely the responsibility of the authors and does not necessarily represent the official views of the National Institutes of Health.

Disclosure: **L.D. Bennett**, None; **M. Klein**, None; **F.T. John**, None; **B. Radojevic**, None; **K. Jones**, None; **D.G. Birch**, None

References

1. Collart FR, Huberman E. Cloning and sequence analysis of the human and Chinese hamster inosine-5'-monophosphate dehydrogenase cDNAs. *J Biol Chem*. 1988;263:15769–15772.
2. Senda M, Natsumeda Y. Tissue-differential expression of two distinct genes for human IMP dehydrogenase (E.C.1.1.1.205). *Life Sci*. 1994;54:1917–1926.
3. Carr SF, Papp E, Wu JC, Natsumeda Y. Characterization of human type I and type II IMP dehydrogenases. *J Biol Chem*. 1993;268:27286–27290.
4. Natsumeda Y, Ohno S, Kawasaki H, Konno Y, Weber G, Suzuki K. Two distinct cDNAs for human IMP dehydrogenase. *J Biol Chem*. 1990;265:5292–5295.
5. Hedstrom L. IMP dehydrogenase: mechanism of action and inhibition. *Curr Med Chem*. 1999;6:545–560.
6. Mortimer SE, Hedstrom L. Autosomal dominant retinitis pigmentosa mutations in inosine 5'-monophosphate dehydrogenase type I disrupt nucleic acid binding. *Biochem J*. 2005;390:41–47.
7. Aherne A, Kennan A, Kenna PF, et al. On the molecular pathology of neurodegeneration in IMPDH1-based retinitis pigmentosa. *Hum Mol Genet*. 2004;13:641–650.
8. Bowne SJ, Sullivan LS, Mortimer SE, et al. Spectrum and frequency of mutations in IMPDH1 associated with autosomal dominant retinitis pigmentosa and leber congenital amaurosis. *Invest Ophthalmol Vis Sci*. 2006;47:34–42.
9. Kozma P, Hughbanks-Wheaton DK, Locke KG, et al. Phenotypic characterization of a large family with RP10 autosomal-dominant retinitis pigmentosa: an Asp226Asn mutation in the IMPDH1 gene. *Am J Ophthal*. 2005;140:858–867.
10. Schatz P, Ponjavic V, Andreasson S, McGee TL, Dryja TP, Abrahamson M. Clinical phenotype in a Swedish family with a mutation in the IMPDH1 gene. *Ophthal Genet*. 2005;26:119–124.
11. Wada Y, Sandberg MA, McGee TL, Stillberger MA, Berson EL, Dryja TP. Screen of the IMPDH1 gene among patients with dominant retinitis pigmentosa and clinical features associated with the most common mutation, Asp226Asn. *Invest Ophthalmol Vis Sci*. 2005;46:1735–1741.
12. Bennett LD, Klein M, Locke KG, Kiser K, Birch DG. Dark-adapted chromatic perimetry for measuring rod visual fields in patients with retinitis pigmentosa. *Transl Vision Sci Technol*. 2017;6:15.
13. Bennett LD, Metz G, Klein M, Locke KG, Khwaja A, Birch DG. Regional variations and intra-/intersession repeatability for scotopic sensitivity in normal controls and patients with inherited retinal degenerations. *Invest Ophthalmol Vis Sci*. 2019;60:1122–1131.

14. Hecht S, Williams RE. The visibility of monochromatic radiation and the absorption spectrum of visual purple. *J Gen Physiol*. 1922;5:1–33.
15. Wald G. On rhodopsin in solution. *J Gen Physiol*. 1938;21:795–832.
16. Wald G. Human vision and the spectrum. *Science*. 1945;101:653–658.
17. Dartnall HJ. Visual purple and the photopic luminosity curve. *The British journal of ophthalmology*. 1948;32:793–811.
18. Wald G, Zeavin BH. Rod and cone vision in retinitis pigmentosa. *Am J Ophthal*. 1956;42:253–269.
19. Gunkel RD. Retinal profiles. A psychophysical test of rod and cone sensitivity. *Arch Ophthalmol*. 1967;77:22–25.
20. Stiles WS, Wyszecki G. Colour-matching data and the spectral absorption curves of visual pigments. *Vision Res*. 1974;14:195–207.
21. Massof RW, Finkelstein D. Rod sensitivity relative to cone sensitivity in retinitis pigmentosa. *Invest Ophthalmol Vis Sci*. 1979;18:263–272.
22. McCulloch DL, Marmor MF, Brigell MG, et al. ISCEV Standard for full-field clinical electroretinography (2015 update). *Doc Ophthalmol Adv Ophthalmol*. 2015;130:1–12.
23. Bowne SJ, Sullivan LS, Blanton SH, et al. Mutations in the inosine monophosphate dehydrogenase 1 gene (IMPDH1) cause the RP10 form of autosomal dominant retinitis pigmentosa. *Hum Mol Genet*. 2002;11:559–568.
24. Birch DG, Anderson JL. Standardized full-field electroretinography. Normal values and their variation with age. *Arch Ophthalmol*. 1992;110:1571–1576.
25. Wada Y, Tada A, Itabashi T, Kawamura M, Sato H, Tamai M. Screening for mutations in the IMPDH1 gene in Japanese patients with autosomal dominant retinitis pigmentosa. *Am J Ophthal*. 2005;140:163–165.
26. Sleiman K, Veerappan M, Winter KP, et al. Optical coherence tomography predictors of risk for progression to non-neovascular atrophic age-related macular degeneration. *Ophthalmology*. 2017;124:1764–1777.
27. Mizukami T, Hotta Y, Katai N. Higher numbers of hyperreflective foci seen in the vitreous on spectral-domain optical coherence tomographic images in eyes with more severe diabetic retinopathy. *Int J Ophthalmol*. 2017;238:74–80.
28. Okuwobi IP, Fan W, Yu C, et al. Automated segmentation of hyperreflective foci in spectral domain optical coherence tomography with diabetic retinopathy. *J Med Imaging (Bellingham)*. 2018;5:014002.
29. Nagasaka Y, Ito Y, Ueno S, Terasaki H. Number of hyperreflective foci in the outer retina correlates with inflammation and photoreceptor degeneration in retinitis pigmentosa. *Ophthalmol Retina*. 2018;2:726–734.
30. Kuroda M, Hirami Y, Hata M, Mandai M, Takahashi M, Kurimoto Y. Intraretinal hyperreflective foci on spectral-domain optical coherence tomographic images of patients with retinitis pigmentosa. *Clin Ophthalmol*. 2014;8:435–440.
31. Bolz M, Schmidt-Erfurth U, Deak G, et al. Optical coherence tomographic hyperreflective foci: a morphologic sign of lipid extravasation in diabetic macular edema. *Ophthalmology*. 2009;116:914–920.
32. Gupta N, Brown KE, Milam AH. Activated microglia in human retinitis pigmentosa, late-onset retinal degeneration, and age-related macular degeneration. *Exp Eye Res*. 2003;76:463–471.
33. Marc RE, Jones BW, Watt CB, Strettoi E. Neural remodeling in retinal degeneration. *Progr Retinal Eye Res*. 2003;22:607–655.
34. Li ZY, Kljavin IJ, Milam AH. Rod photoreceptor neurite sprouting in retinitis pigmentosa. *J Neurosci*. 1995;15:5429–5438.
35. Bergstrom R, Czyz CN. Vitreous floaters. *StatPearls*. 2019.
36. Cabral T, Sengillo JD, Duong JK, et al. Retrospective analysis of structural disease progression in retinitis pigmentosa utilizing multimodal imaging. *Sci Rep*. 2017;7:10347.
37. Sujirakul T, Lin MK, Duong J, Wei Y, Lopez-Pintado S, Tsang SH. Multimodal imaging of central retinal disease progression in a 2-year mean follow-up of retinitis pigmentosa. *Am J Ophthal*. 2015;160:786–798 e784.
38. Jauregui R, Takahashi VKL, Park KS, et al. Multimodal structural disease progression of retinitis pigmentosa according to mode of inheritance. *Sci Rep*. 2019;9:10712.
39. Puck A, Tso MO, Fishman GA. Drusen of the optic nerve associated with retinitis pigmentosa. *Arch Ophthalmol*. 1985;103:231–234.
40. Edwards A, Grover S, Fishman GA. Frequency of photographically apparent optic disc and parapapillary nerve fiber layer drusen in Usher syndrome. *Retina*. 1996;16:388–392.
41. Nischal KK, Hingorani M, Bentley CR, et al. Ocular ultrasound in Alagille syndrome: a new sign. *Ophthalmology*. 1997;104:79–85.
42. White RJ, Watson DJ, Koozekanani DD, Montezuma SR. Association of optic nerve head drusen with best vitelliform macular dystrophy: a case series. *Case Rep Ophthalmol*. 2018;9:76–86.

43. Silverman AL, Tatham AJ, Medeiros FA, Weinreb RN. Assessment of optic nerve head drusen using enhanced depth imaging and swept source optical coherence tomography. *J Neuro-ophthalmol*. 2014;34:198–205.
44. Fingeret M, Medeiros FA, Susanna R, Jr., Weinreb RN. Five rules to evaluate the optic disc and retinal nerve fiber layer for glaucoma. *Optometry*. 2005;76:661–668.
45. Sawada Y, Hangai M, Ishikawa M, Yoshitomi T. Association of myopic optic disc deformation with visual field defects in paired eyes with open-angle glaucoma: a cross-sectional study. *PloS One*. 2016;11:e0161961.
46. Jacobson SG, Buraczynska M, Milam AH, et al. Disease expression in X-linked retinitis pigmentosa caused by a putative null mutation in the RPGR gene. *Invest Ophthalmol Vis Sci*. 1997;38:1983–1997.
47. Jacobson SG, Roman AJ, Cideciyan AV, Robey MG, Iwata T, Inana G. X-linked retinitis pigmentosa: functional phenotype of an RP2 genotype. *Invest Ophthalmol Vis Sci*. 1992;33:3481–3492.
48. Grover S, Fishman GA, Birch DG, Locke KG, Rosner B. Variability of full-field electroretinogram responses in subjects without diffuse photoreceptor cell disease. *Ophthalmology*. 2003;110:1159–1163.
49. Aherne A, Kennan A, Kenna PF, McNally N, Farrar GJ, Humphries P. Molecular mechanisms of photoreceptor degeneration in RP caused by IMPDH1 mutations. *Adv Exp Med Biol*. 2006;572:81–87.
50. Bowne SJ, Liu Q, Sullivan LS, et al. Why do mutations in the ubiquitously expressed housekeeping gene IMPDH1 cause retina-specific photoreceptor degeneration? *Invest Ophthalmol Vis Sci*. 2006;47:3754–3765.
51. Li M, Jia C, Kazmierkiewicz KL, et al. Comprehensive analysis of gene expression in human retina and supporting tissues. *Hum Mol Genet*. 2014;23:4001–4014.
52. Huang F, Ni M, Chalishazar MD, et al. Inosine monophosphate dehydrogenase dependence in a subset of small cell lung cancers. *Cell Metab*. 2018;28:369–382, e365.
53. McCune JS, Storer B, Thomas S, McKiernan J, Gupta R, Sandmaier BM. Inosine monophosphate dehydrogenase pharmacogenetics in hematopoietic cell transplantation patients. *Biol Blood Marrow Transplant*. 2018;24:1802–1807.
54. Cao W, Xiao H, Lai X, et al. Genetic variations in the mycophenolate mofetil target enzyme are associated with acute GVHD risk after related and unrelated hematopoietic cell transplantation. *Biol Blood Marrow Transplant*. 2012;18:273–279.
55. Okour M, Jacobson PA, Ahmed MA, Israni AK, Brundage RC. Mycophenolic acid and its metabolites in kidney transplant recipients: a semimechanistic enterohepatic circulation model to improve estimating exposure. *J Clin Pharmacol*. 2018;58:628–639.

Amended May 18, 2020: In the author affiliations, the city and state listed for University of Oklahoma Health Sciences Center was changed from Dallas, TX, to Oklahoma City, OK.